scientific reports

OPEN

Study of repulsive permanent magnetic levitation mechanism and its dynamic characteristics

Fazhu Zhou[1,2], Jie Yang[1,2]✉, Hailin Hu[1,2] & Tao Gao[1,2]

Permanent magnet magnetic levitation (PMFL) system has the characteristics of zero-power levitation, strong load-carrying capacity and self-stabilization, so it has obvious advantages in the application of rail transportation and heavy-duty transmission and other fields. However, due to the lack of active control of electromagnetism and the existence of multi-point coupling, it is easily affected by external factors, and its dynamic characteristics and its complexity. This paper aims to reveal the levitation mechanism of permanent magnet magnetic levitation system and the coupling motion law of bogie by combining theoretical analysis and experimental verification. Firstly, the proportional and exponential correction coefficients for the magnetic induction strength are introduced to establish an analytical model for the levitation force. Secondly, the three-dimensional dynamic characteristic model of the bogie is established by analyzing the running attitude and external disturbing factors, revealing the four-point levitation coupling mechanism, and judging its stability by using the motion control theory. On this basis, input and output decoupling is realized by the method of coordinate transformation. Finally, through simulation analysis and physical experiments, the bogie motion law under various complex working conditions is explored, and the validity and reliability of the research is proved.

The development and application of magnetic levitation technology has prompted the speed of rail transportation to constantly achieve new breakthroughs. Compared with the traditional wheeled rail transportation, the maglev train has a greater improvement in running speed and comfort, making an important contribution to the improvement of the quality of human transportation. Permanent magnetic suspension (PMS), as a kind of levitation, has the advantages of ultra-low levitation energy consumption and self-stabilized levitation without complex control system[1–3]. In order to explore the mechanism of PMS, master the motion law of PMS and promote the development of PMS technology, scholars at home and abroad have carried out a series of research on PMS technology and accumulated some research results[4–7].

At present, the research of permanent magnet levitation system mainly focuses on the model analysis of permanent magnet levitation force and structural optimization of the two technical routes, the former is through the establishment of levitation force mathematical model to explore the physical relationship between levitation force and the spatial structure of permanent magnets, and the latter tends to optimize the spatial structure of permanent magnets and magnetization direction by combining with the optimization theory and the design of the magnetic circuit to improve the levitation efficiency of the permanent magnets. Pei Wenzhe et al.[8–10]. proposed a variable magnetic circuit type permanent magnetic levitation platform with low power consumption and anti-adsorption, and designed a three-degree-of-freedom centralized control method for the levitation tilt problem, and finally verified its validity through experiments. Ye Hong et al. used the Nelder-Mead Simplex method (NMS) in the optimization solver of COMSOL software to optimize the geometrical parameters of the HALBACH permanent magnet generator (PMG) according to the different objective requirements of the HTS magnetic levitation system and demonstrated that this method can improve the utilization of the magnetic field.[11]. In order to enhance the floating weight ratio, the American scientist Klaus HALBAC[12] proposed a new type of permanent magnet arrangement Halbach array, will be different from the direction of magnetization of permanent magnets arranged in a certain order to make the array on one side of the magnetic field to strengthen the magnetic field of the other side of the magnetic field is significantly weakened, as shown in Fig. 1, this characteristic in the field of permanent magnet motors and magnetic levitation mass transit have a wide range

[1]School of Electrical Engineering and Automation, Jiangxi University of Science and Technology, Ganzhou 341000, China. [2]Jiangxi Provincial Key Laboratory of Maglev Rail Transit Equipment, Ganzhou 341100, China. ✉email: 15405993@qq.com
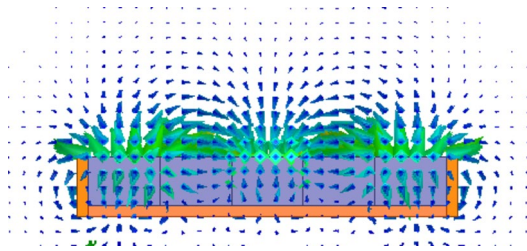
Fig. 1. Magnetic field distribution of Halbach array.

Fig. 2. "Red Track. Xingguo" permanent magnetic levitation project demonstration line.

of prospects for application. Jiang Xin et al.[13] proposed an odd/even segmented pole structure for Halbach permanent magnet arrays, analyzed the analytical model and optimized parameter calculations, and applied it to linear motors. Haopeng Jia et al., modelled a high-temperature superconducting permanent magnetic levitation (PML) system based on Maxwell's system of equations and compared it with experimental data, thus finding that the levitation and guiding forces of a high-temperature superconducting PML system decrease regularly as the defects are enlarged, which leads to a decrease in the load-carrying capacity and stability of the system[14]. Chen Junhui et al.[15,16] established a mathematical model of radial magnetic force of Halbach array permanent magnetic bearing based on the molecular current method, and verified the accuracy of the model by combining with the finite element method. Hongfu Shi et al.[17]. investigated the dynamic electromagnetic characteristics and thermo-mechanical coupling effects of a linear permanent magnet electrodynamic suspension system (PMEDS) by means of a high-speed test rig, and explored the velocity characteristics and vertical vibration law of the test rig. Chunsheng Li et al.[18] proposed optimization indexes for linear Halbach magnet levitation structure, gave optimization results through analysis, and verified experimentally. Fang Haifeng et al.[19] studied the effect of each size parameter of permanent magnet on levitation force through numerical simulation and finite element analysis, and optimized the structural size parameter of the magnet unit based on the multi-island genetic method, so as to improve the magnetic energy utilization.

The continuous updating and iteration of permanent magnet magnetic levitation (PMMLEV) technology has led to new breakthroughs in the field of rail transportation. Li Lingqun[20] proposed a permanent magnet compensated magnetic levitation (PMCML) technology, which utilizes the principle of mutual compensation between the repulsive force of the permanent magnet material and the suction working mechanism to make the train levitate stably, and developed a permanent magnet magnetic levitation (PMMLEV) train with a width of 3.12 m and a height of 2.86 m, which can carry 32 people, and is named as the " Zhonghua 01". Israeli scientists such as WISEMAN[21,22] proposed a permanent magnetic array mutual exclusion levitation with high-speed, energy-saving, convenient inner-city small-scale magnetic levitation transportation system, and named it "Sky Tran" has attracted wide attention. Based on the principle of homogeneous rejection of Halbach array, Yang Jie et al.[23,24] proposed a permanent magnetic levitation (PML) rail transportation system—"Red Rail", which has the characteristics of low magnetic levitation energy consumption, low operation and maintenance, greenness, safety, intelligence, etc., and completed the construction of the PML test line and the engineering demonstration line, as shown in Fig. 2.

Although permanent magnetic levitation (PML) has many advantages and has accumulated rich research results, PML system is a typical complex controlled system with multi-modal and multi-degree-of-freedom motions. Its levitation and guidance there is a more complex coupling relationship, permanent magnetic levitation technology towards engineering applications still face multiple challenges. For example, self-excited oscillations are easily generated in the under-damped state, and the repulsive Halbach array levitation structure has strong nonlinearities and negative guidance, which to a certain extent hinders the engineering application of permanent magnet magnetic levitation (PM levitation) technology. The main work of this paper is specified as follows:

1. Introducing the proportional and exponential correction factor of magnetic induction strength to establish its vertical magnetic force analytical model based on halbach array, and exploring the mechanism of permanent magnet magnetic levitation.

2. On the basis of the single-point permanent magnetic force analytical model, the three-dimensional dynamic characteristic model of the bogie is established by analyzing the operating attitude of the bogie and external interference factors, which reveals the coupling mechanism of the rigid permanent magnetic levitation bogie.

3. The input and output of the rigid bogie are decoupled by the method of coordinate transformation, and the bogie motion law of the permanent magnetic levitation support system under complex working conditions is explored through simulation and physical experiment.

Levitation force model

In order to explore the Halbach array permanent magnetic levitation system levitation force and levitation gap, magnet performance and its structural size parameters and other effects on the levitation force, the red rail R & D team JIANG et al.[25] designed a repulsive levitation frame by using Halbach arrays, and reasoned out the three sets of Halbach array levitation force mathematical model. However, the results of simulation and experiment show that the use of five groups of Halbach array repulsive levitation structure is better than three groups of Halbach array levitation efficiency and carrying capacity. In engineering practice permanent magnet magnetic levitation systems are usually installed with mechanical guide wheels to increase friction damping and complete the guiding function to achieve self-stabilized levitation. In this paper, we propose to use a 5-group Halbach array rejection levitation structure to establish its levitation force mathematical model, and its levitation structure is shown in Fig. 3.

The reinforced side magnetic induction[26] of the Halbach array permanent magnet group can be expressed as

$$\begin{cases} B_0 = \dfrac{B_r k_1 (1-e^{-kd}) \sin(\frac{\pi}{n})}{\pi/n} \\ B_x = B_0 \sin(kx) e^{-kk_2 z} \\ B_z = B_0 \cos(kx) e^{-kk_2 z} \end{cases} \tag{1}$$

In (1), B_0 is the magnetic induction intensity on the reinforced side, B_x and B_z are the components of the magnetic induction intensity along the X-axis and Z-axis on the reinforced side of the Halbach array, B_r is the remanent magnetization of the permanent magnet, k is the number of wavelengths of the Halbach array magnetic group, $k = 2\pi/\lambda$, λ is the wavelength of the permanent magnet and $\lambda = nw$, n is the number of magnetic blocks per unit wavelength, z is the levitation air gap, w is the width of the unit magnetic block, d is the thickness of the permanent magnet, k_1 and k_2 are the correction factors for the magnetic induction intensity. According to the results of literature[26], the levitation force along the z-axis of the reinforced side of a single levitation module when $n = 4$ can be expressed as follows

$$F = \frac{10k_1^2 B_r^2 wl \left(1 - e^{-kd}\right)^2 e^{-2kk_2 z}}{\pi^2 \mu_0} \tag{2}$$

In (2), F is the levitation force of the parallel Halbach module and   is the length of the vehicle magnet in the y-axis direction.

Equation (2) basically reflects the relationship between the spatial dimensions of the symmetric Halbach levitation structure and the levitation force. By introducing the proportional correction coefficient k_1 and the exponential correction coefficient k_2 of the magnetic field strength, and combining the analog simulation and physical measurements to determine the values of k_1 and k_2, we can ensure that the analytical model of the levitation force is accurate and reliable.

In order to compare the pre-correction and post-correction models, Table 1 is presented. Compared with the original uncorrected model proposed in reference[18], the improved model significantly enhances the accuracy of the model through the strategy of integrating the proportional correction factor k_1 and the exponential correction factor k_2. Specifically, the introduced proportional correction factor effectively compensates for the
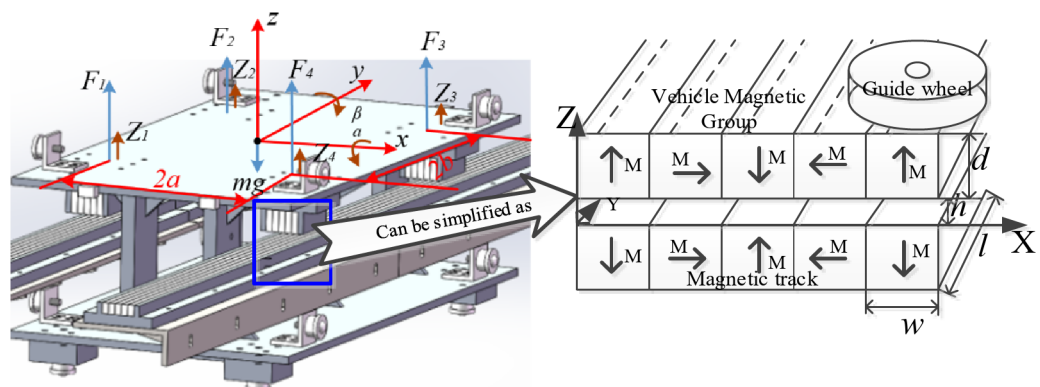

Fig. 3. Permanent magnetic levitation struct.

Non-refined models[18]	Refined models
$F = \frac{5}{2} \frac{B_r^2 \lambda l \left(1 - e^{-kd}\right)^2 e^{-2kz}}{\pi^2 \mu_0}$	$F = \frac{10k_1^2 B_r^2 wl \left(1 - e^{-kd}\right)^2 e^{-2kk_2 z}}{\pi^2 \mu_0}$

Table 1. Relevant model parameters.

bias caused by the differences in the properties of different permanent magnet materials, while the inclusion of the exponential correction factor successfully mitigates the uncertainty caused by the fluctuations in the mounting accuracy of the suspension module, which ensures that the constructed model can be widely adapted to diverse and complex working conditions.

Expanding (2) using the Taylor series method and omitting the higher order terms, the linearized levitation force is given as

$$F_{\mathrm{n}} = F_n(z_0) + F'_{n-z}(z_0)\Delta z \tag{3}$$

In (3), F_n ($n = 1, 2, 3, 4$) is the levitation force, $F_n(z_0)$ is the levitation force at the equilibrium point, and $F'_{n-z}(z_0)$ is expressed in (4).

$$F'_{\mathrm{n}-z}(z_0) = -\frac{20kk_2 k_1^2 B_r^2 wy \left(1 - e^{-kd}\right)^2 e^{-2kk_2 z_0}}{\pi^2 \mu_0} \tag{4}$$

Kinetic modeling

The analysis of the dynamics model helps the system optimization design and control strategy selection, and also predicts the response and motion trajectory of the system under different initial conditions and external disturbances, thus contributing to the performance evaluation, parameter optimization and design verification. However, the permanent magnet magnetic levitation (PMML) system with rigid bogie has the problems of variable lateral force and multi-point coupling, and its motion law is complex and variable. Therefore, it becomes an urgent problem to reveal the mechanism of permanent magnetic levitation and the motion law of the bogie by establishing an accurate dynamic model.

In this paper, the dynamics is modeled with the bogie with permanent magnetic levitation shown in Fig. 3 and the following assumptions are made:

1. Assuming that the machining and assembly precision of the steel structure body of the permanent magnet magnetic levitation (PMML) bogie, the magnetic track, and the guide wheel are sufficient and error-free, and that the center of mass is at the center of the bogie, the pitching motion and the side tilting motion of the bogie are centered on the x and y axes, respectively.
2. It is assumed that all mechanical structures of box girders, magnetic tracks, and bogies are rigid.
3. Assuming that the magnetic material has a uniform and stable permeability, coercivity, and ignoring the effects of temperature, humidity, light, etc.
4. Assuming that the damping coefficients of the bogie in the three degrees of freedom do not change during the levitation process, and ignoring the magnetic force changes caused by the tiny side deviation or small angle pitching motion of the levitation module.

As shown in Fig. 3, the motion of the bogie can be regarded as the superposition of three degrees of freedom: the vertical motion along the z-axis, the pitch motion around the x-axis, and the lateral tilt motion around the y-axis. According to the laws of motion mechanics, the dynamics model of the three degrees of freedom of the bogie can be established as follows:

$$\begin{cases} m\ddot{z} = (F_1 + F_2 + F_3 + F_4) - mg - c_1\dot{z} + f_{dz}(t) \\ J_\alpha \ddot{\alpha} = (-F_1 + F_2 + F_3 - F_4)a - c_2\dot{\alpha} + f_{d\alpha}(t) \\ J_\beta \ddot{\beta} = (F_1 + F_2 - F_3 - F_4)b - c_3\dot{\beta} + f_{d\beta}(t) \end{cases} \tag{5}$$

In (5), m i is the weight of the permanent magnetic levitation (PML) bogie, g is the acceleration of gravity, J_α and J_β are the rotational inertia of the bogie around the x-axis and the y-axis, respectively; z, α, β are the displacements and inclinations of the bogie in three degrees of freedom during levitation process, respectively; F_1, F_2, F_3, F_4 are the levitation forces of the four poles of the bogie, respectively; b and a are the distances between the poles along the x-axis and y-axis and the centerline of the bogie, and c_1, c_2, c_3 are the damping coefficients in the three degrees of freedom, and $f_{dz}(t)$, $f_{d\alpha}(t)$, $f_{d\beta}(t)$ are the perturbations on the three degrees of freedom z, α, β, respectively.

The equilibrium condition for the three degrees of freedom is

$$\begin{cases} F_1(z_0) + F_2(z_0) + F_3(z_0) + F_4(z_0) = mg \\ -F_1(z_0) + F_2(z_0) + F_3(z_0) - F_4(z_0) = 0 \\ F_1(z_0) + F_2(z_0) - F_3(z_0) - F_4(z_0) = 0 \end{cases} \tag{6}$$

Bringing (3) and (6) into (5) yields

$$\begin{cases} m\ddot{z} = F'_{1-z}(z_0)\Delta z_1 + F'_{2-z}(z_0)\Delta z_2 + F'_{3-z}(z_0)\Delta z_3 + F'_{4-z}(z_0)\Delta z_4 - c_1\dot{z} + f_{dz}(t) \\ J_\alpha\ddot{\alpha} = [-F'_{1-z}(z_0)\Delta z_1 + F'_{2-z}(z_0)\Delta z_2 + F'_{3-z}(z_0)\Delta z_3 - F'_{4-z}(z_0)\Delta z_4]a - c_2\dot{\alpha} + f_{d\alpha}(t) \\ J_\beta\ddot{\beta} = [F'_{1-z}(z_0)\Delta z_1 + F'_{2-z}(z_0)\Delta z_2 - F'_{3-z}(z_0)\Delta z_3 - F'_{4-z}(z_0)\Delta z_4]b - c_3\dot{\beta} + f_{d\beta}(t) \end{cases} \quad (7)$$

According to (7) the kinetic linear differential equation can be written in matrix form as shown in (8).

$$M \begin{bmatrix} \ddot{z} \\ \ddot{\alpha} \\ \ddot{\beta} \end{bmatrix} = F'_{n-z}(z_0)N \begin{bmatrix} \Delta z_1 \\ \Delta z_2 \\ \Delta z_3 \\ \Delta z_4 \end{bmatrix} - C \begin{bmatrix} \dot{Z} \\ \dot{\alpha} \\ \dot{\beta} \end{bmatrix} + \begin{bmatrix} f_{dz}(t) \\ f_{d\alpha}(t) \\ f_{d\dot{\beta}}(t) \end{bmatrix} \quad (8)$$

In (8), M is the inertia matrix of the system, C is the damping matrix of the system, and N is the differential matrix of the system, which are expressed as follows, respectively:

$$M = \begin{bmatrix} m & & \\ & J_\alpha & \\ & & J_\beta \end{bmatrix}, \quad C = \begin{bmatrix} c_1 & & \\ & c_2 & \\ & & c_3 \end{bmatrix} \quad N = \begin{bmatrix} 1 & 1 & 1 & 1 \\ -a & a & a & -a \\ b & b & -b & -b \end{bmatrix} \quad (9)$$

The four-magnet pole permanent magnetic levitation system is a typical multi-input and multi-output system, due to the lack of electromagnetic active control, when perturbed, the bogie simultaneously exists in the pendant, pitch and side tilt three degrees of freedom, and the displacement change rules of different magnetic poles are different, resulting in a complex and changeable system motion law. When the perturbation of the system is used as the input and the displacement of each magnetic pole is used as the output, according to the analysis of (8), the system can be regarded as a three-input and four-output system under the state of non-decoupling, where the inputs and outputs lack the direct correspondence, so it is more difficult to analyze the motion law of the bogie when the system is subjected to different perturbations. Specifically, when the displacement of one pole changes, the displacements of the other poles also change to maintain the stability of the system.

Stability and decoupling analysis

In order to analyze the stability of the system and the coupling relationship between the four magnetic poles, the dynamical equations of the system are determined by establishing the coordinate change relationship between the vertical displacement of the four magnetic poles and the displacement and inclination of the three-degree-of-freedom motions, and associating them with the dynamical equations of the system. On this basis, the stability and coupling relationship of the system are analyzed.

According to Fig. 3, the coordinate variation schematic diagrams of the bogie pitching motion and side tilting motion can be drawn, as shown in Fig. 4.
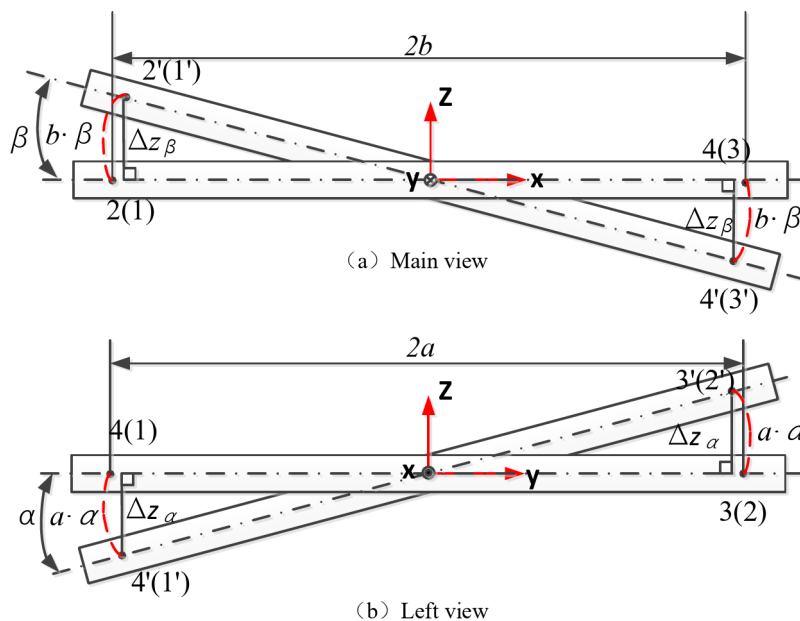

(a) Main view

(b) Left view

Fig. 4. Schematic diagram of magneto-polar coordinate transformation.

As shown in Fig. 4(a), when the lateral inclination angle of the levitated platform clockwise around the y-axis is β, the magnetic pole 1 moves from point 1 to point $1'$, and its arc trajectory length is $b\cdot\beta$, and the vertical displacement is $z_{1\beta} = b \cdot \sin\beta$. In addition, when the overall vertical displacement of the levitated platform is z, the vertical displacement of pole 1 will be $z_{1z} = z$. As shown in Fig. 5(b), when the counterclockwise pitch angle of the bogie around the x-axis is α, magnetic pole 1 moves from point 1 to point $1'$, and the length of its arc trajectory is $a\cdot\alpha$, while its vertical displacement is $z_{1\alpha} = -a.\sin\alpha$.

The change of vertical displacement of magnetic pole 1 can be expressed as $\Delta z_1 = z_{1z} + z_{1\alpha} + z_{1\beta} = z - a \cdot \sin\alpha + b \cdot \sin\beta$. In the actual levitation and motion control process, the pitch and side tilt motions of the magnetic levitation platform are small, so $\sin\alpha \approx \alpha, \sin\beta \approx \beta (\alpha, \beta \approx 0)$,$\Delta z_1 = z - a\alpha + b\beta$.

Similarly, the change in vertical displacement of magnetic poles 1–4 can be expressed as Δz_n

$$\begin{cases} \Delta z_1 = z - a\alpha + b\beta \\ \Delta z_2 = z + a\alpha + b\beta \\ \Delta z_3 = z + a\alpha - b\beta \\ \Delta z_4 = z - a\alpha - b\beta \end{cases} \tag{10}$$

(10) can be written in matrix form as

$$\begin{bmatrix} \Delta z_1 & \Delta z_2 & \Delta z_3 & \Delta z_4 \end{bmatrix}^T = N_1 \begin{bmatrix} z & \alpha & \beta \end{bmatrix}^T \tag{11}$$

Let $N_2 N_1 = E_{3\times 3}$, according to (11) we have

$$\begin{bmatrix} z & \alpha & \beta \end{bmatrix}^T = N_2 \begin{bmatrix} \Delta z_1 & \Delta z_2 & \Delta z_3 & \Delta z_4 \end{bmatrix}^T \tag{12}$$

where $N_1 = N^T$ is the coordinate inversion matrix and N_2 is the coordinate inverse transformation matrix; its specific form is shown as follows.
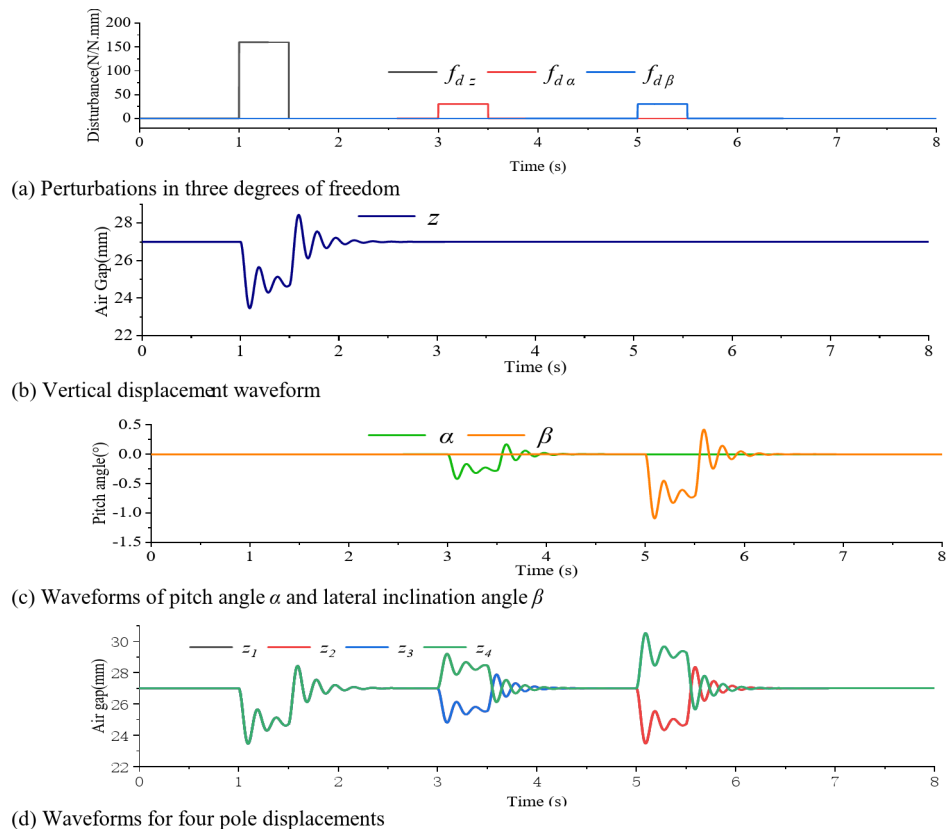

(a) Perturbations in three degrees of freedom

(b) Vertical displacement waveform

(c) Waveforms of pitch angle α and lateral inclination angle β

(d) Waveforms for four pole displacements

Fig. 5. Input–output decoupling simulation waveforms.

$$N_1 = \begin{bmatrix} 1 & -a & +b \\ 1 & +a & +b \\ 1 & +a & -b \\ 1 & -a & -b \end{bmatrix}, \quad N_2 = \frac{1}{4}\begin{bmatrix} 1 & 1 & 1 & 1 \\ -\frac{1}{a} & \frac{1}{a} & \frac{1}{a} & -\frac{1}{a} \\ \frac{1}{b} & \frac{1}{b} & -\frac{1}{b} & -\frac{1}{b} \end{bmatrix} \tag{13}$$

(11) and (12) are the vertical displacements of the four magnetic poles of the bogie versus the coordinate changes of the three degrees of freedom.

Bringing (11) into (8) and collapsing, the linear dynamics equation of the system can be obtained as shown in (14).

$$\begin{bmatrix} \ddot{z} \\ \ddot{\alpha} \\ \ddot{\beta} \end{bmatrix} + M^{-1}C\begin{bmatrix} \dot{Z} \\ \dot{\alpha} \\ \dot{\beta} \end{bmatrix} - F'_{n-z}(z_0)M^{-1}NN_1\begin{bmatrix} Z \\ \alpha \\ \beta \end{bmatrix} - M^{-1}\begin{bmatrix} f_{dz} \\ f_{d\alpha} \\ f_{d\dot{\beta}} \end{bmatrix} = 0 \tag{14}$$

In (14), it is easy to know that all the coefficients of $F'_{n-z}(z_0)M^{-1}NN_1$ are <0 by substituting the parameters, and when the coefficients of the damping matrix C are positive, the real part of all the eigenroots of the system is negative, and the system can be judged to be self-stabilizing. When the bogie is stabilized near the equilibrium position (both $\ddot{z}, \dot{z}, \ddot{\alpha}, \dot{\alpha}, \ddot{\beta}, \dot{\beta}$ are equal to zero), the vertical displacement z of the bogie is linearly related to the perturbation of the three degrees of freedom. The expression of NN_1 is shown in (15).

$$NN_1 = \begin{bmatrix} 4 & 0 & 0 \\ 0 & 4a^2 & 0 \\ 0 & 0 & 4b^2 \end{bmatrix} \tag{15}$$

The permanent magnetic levitation system has a self-stabilizing nature, but in the under-damped state, the motion of the bogie is affected by the health state of the magnetic track, installation accuracy, load variation, etc., which is prone to generate self-excited oscillatory motion, as shown in (14). After solving by using the coordinate transformation matrix, the prefix matrix NN1 in the mathematical model of the maglev platform has been transformed into a diagonal matrix, i.e., the motion of each degree of freedom of the platform uniquely corresponds to the perturbation of the three degrees of freedom. Therefore, it can be inferred that the method can be used for input–output decoupling of the system. Theoretically, the actual system can realize the decoupling of the perturbation of the three degrees of freedom of the levitated platform and the displacement of each magnetic pole by inversely solving the equivalent displacement of each magnetic pole by the method shown in (11). Based on this method, it can be used for motion control, system design, performance improvement and other research work of the permanent magnetic levitation system.

Simulation

The system is transformed into a second-order, three-input, three-output system by taking $f_{dz}, f_{d\alpha}, f_{d\beta}$ as the inputs of the system and z, α, β as the outputs of the system. Therefore, the expressions for the input variable u and the output variable y of the state space equation are shown in (16). Taking the state variable x of the system as shown in (17), the first order state variable $\dot{x}$ of the system is shown in (18). Combining the above variables, the state space equation of the system can be determined according to (14) as shown in (19).

$$u = \begin{bmatrix} f_{dz} & f_{d\alpha} & f_{d\beta} \end{bmatrix}^T, \quad y = \begin{bmatrix} z & \alpha & \beta \end{bmatrix}^T \tag{16}$$

$$x = \begin{bmatrix} z & \alpha & \beta & \dot{z} & \dot{\alpha} & \dot{\beta} \end{bmatrix}^T \tag{17}$$

$$\dot{x} = \begin{bmatrix} \dot{z} & \dot{\alpha} & \dot{\beta} & \ddot{z} & \ddot{\alpha} & \ddot{\beta} \end{bmatrix}^T \tag{18}$$

$$\begin{cases} \dot{x} = Ax + Bu \\ y = Cx \end{cases} \tag{19}$$

In (19), A is the system state matrix, B is the system input matrix, and C is the system output matrix, which is expressed as (20)-(21).

$$A = \begin{bmatrix} 0_{3\times3} & E_{3\times3} \\ M^{-1}F'_{n-z}(z_0)NN_1 & -M^{-1}C \end{bmatrix}$$
$$= \begin{bmatrix} 0_{3\times3} & & & E_{3\times3} & & \\ \frac{4}{m}F'_Z(Z_0) & 0 & 0 & -\frac{c_1}{m} & 0 & 0 \\ 0 & \frac{4a^2}{m}F'_Z(Z_0) & 0 & 0 & -\frac{c_2}{J_\alpha} & 0 \\ 0 & 0 & \frac{4b^2}{m}F'_Z(Z_0) & 0 & 0 & -\frac{c_3}{J_\beta} \end{bmatrix} \tag{20}$$

$$B = \begin{bmatrix} 0_{3\times3} \\ M^{-1} \end{bmatrix} = \begin{bmatrix} 0_{3\times3} \\ \frac{1}{m} & 0 & 0 \\ 0 & \frac{1}{J_\alpha} & 0 \\ 0 & 0 & \frac{1}{J_\beta} \end{bmatrix}, \quad C = \begin{bmatrix} E_{3\times3} & 0_{3\times3} \end{bmatrix} \qquad (21)$$

Substituting the values from Table 2 into (18), the simulation of the dynamic characteristics of the bogie is simulated and analyzed in the following four steps.

Step 1 Input–output decoupling verification.

In order to verify that the input and output decoupling of the bogie can be realized by using the coordinate transformation method, the step perturbation signals shown in Fig. 5(a) are applied to the three degrees of freedom of the bogie at the moments of 1 s, 3 s, and 5 s, which last for 0.5 s, and the amplitude of the perturbation in the vertical direction is 160N, and the amplitude of the perturbation in the pitch and lateral inclination directions is 30 N.mm. The vertical displacement of the bogie, z, the pitch angle, α, and lateral inclination, β, and the air gap data of the four magnetic poles are collected as shown in Fig. 5.

As shown in (b) and (c) of Fig. 5, no perturbation is applied during the 0-1 s period, during which the bogie's vertical displacement, pitch angle and lateral inclination are at the initial position, with z of 27 mm and pitch and lateral inclination of 0°. At the 1 s moment only a vertical step perturbation force of 160 N was applied for 0.5 s. During the 1-3 s period only z shuddered with the applied perturbation, with a minimum of 26.42 mm, while α and β were always maintained at 0°. At the 3 s moment, only 30 N .mm of perturbation torque in the α direction was applied, and only α showed jitter during the 3-5 s period, while z and β were maintained at their initial positions. At the 5 s moment, only 30N .mm perturbation torque in the β direction was applied, and during the 5-7 s period, only β showed jitter while z and α were maintained at the initial position. The simulation results show that the input–output decoupling of the repulsive permanent magnet magnetic levitation system can be realized by the method of coordinate transformation.

Step 2 Magnetic Pole Perturbation Analysis.

In order to explore the effect of perturbation of different magnetic poles on the dynamic characteristics of the bogie, a perturbation force with an amplitude of 16 N was applied to the four magnetic poles at the moments of 1 s, 3 s, 5 s and 7 s, respectively, for a duration of 0.5 s, as shown in Fig. 6(a). The z, α, β of the bogie and the suspended air gaps z_1, z_2, z_3, z_4 of the four magnetic poles are collected as shown in Fig. 6.

As shown in Fig. 6, the oscillation frequencies of α and β are the same while perturbations are applied to the four poles, but the oscillation amplitudes of β are all larger than those of α. During 0-1 s, no perturbation was applied and z, α, β and z_1, z_2, z_3, z_4 were maintained at the initial positions ($z = 27$ mm,$\alpha = 0°$, $\beta = 0°$, $z_1 = z_2 = z_3 = z_4 = 0$ mm). During the period of 1-3 s, the perturbation is applied only in magnetic pole 1. During this period, a small amplitude oscillation of z occurs, which is stabilized after about 1.2 s, with α increasing and then oscillating, and β decreasing and then oscillating. Due to the existence of occasional relationship between the four magnetic poles in the rigid bogie, z_1 and z_2 decrease first and then oscillate, while z_3 and z_4 increase first and then oscillate, and the oscillation amplitudes are z_1, z_3, z_2, and z_4 in the order of largest to smallest. z_1 has a minimum value of about 23.39 mm, z_2 has a minimum value of about 25.34 mm, z_3 has a maximum value of about 30.42 mm, and z_4 has a maximum value of about 28.47 mm or so. During the period of 3-5 s, both α and β decrease and then oscillate, z_1 and z_2 decrease and then oscillate, while z_3 and z_4 increase and then oscillate,

Parameter	Symbol	Value
Thickness of magnetic block	d	20 mm
Length of vehicle magnet	l	100 mm
Unit magnetic block width	w	12 mm
Residual magnetism	B_r	1.35 T
Space permeability	μ_0	$4\pi \times 10^{-7}$H/m
Relative permeability	μ_r	1
Coercivity	H_c	980KA/m
Unit wavelength Number of magnetic blocks	n	4
Proportional correction factor	k_1	0.04935
Exponential correction factor	k_2	0.4424
vertical damping	c_1	654.1872 kg/s
Pitch motion damping	c_2	676.4173 kg.m^2/s
Sway motion damping	c_3	733.8691 kg.m^2/s
Moment of inertia (X-axis)	J_α	5.9199
Moment of inertia (Y-axis)	J_β	2.1441
Weight	m	64.379 kg
Balancing air gap	Z_0	27.23 mm
Distance between magnetic poles 1 (3) and 2 (4)	a	300 mm
Distance between magnetic poles 2(1) and 3(4)	b	185 mm

Table 2. Relevant model parameters.

(a) Quadrupole Input Disturbance Waveforms

(b) Vertical displacement waveform

(c) Waveforms of pitch angle α and lateral inclination angle β
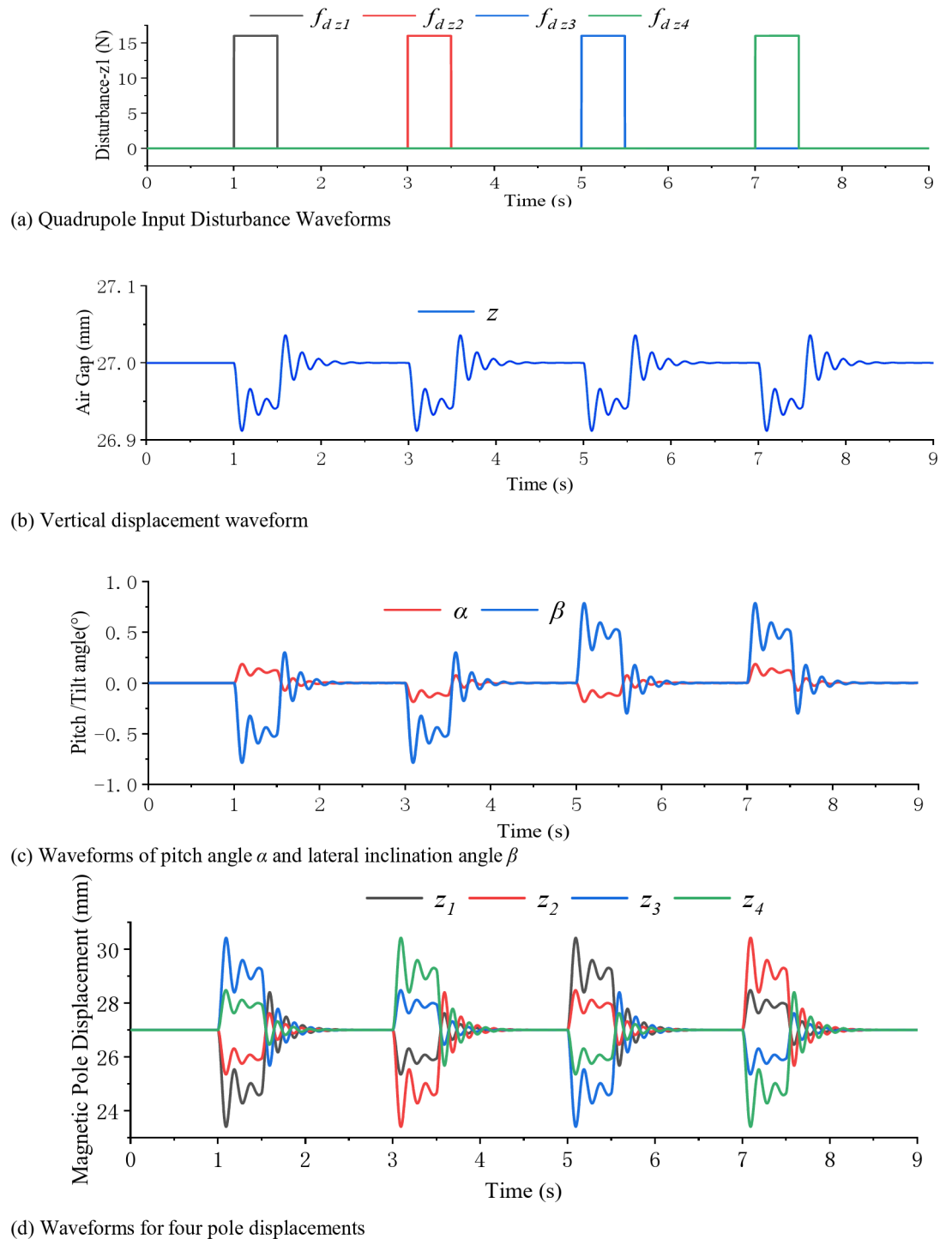

(d) Waveforms for four pole displacements

Fig. 6. Waveforms under 4-pole input perturbation.

and the order of the oscillation amplitude is z_2, z_4, z3, z_1 in the order of largest to smallest. during the period of 5-7 s, α decreases and then oscillates, β increases and then oscillates, z_1 and z_2 increase and then oscillate, while z_3 and z_4 decrease and then oscillate, and the order of oscillation amplitude is z_3, z_4, and z_1 in the order of largest to smallest. The order of oscillation amplitude from largest to smallest is z_3, z1, z_4, z_2. During 7-9 s, both α and β increase and then oscillate, but β oscillates more than α. z_1 and z_2 rise and then oscillate, while z_3 and z_4 fall and then oscillate, and the order of oscillation amplitude from largest to smallest is z_4, z_2, z_1, z_3.

Step 3 Simulation analysis under multiple magnetic pole perturbations.

In order to explore the dynamic characteristics of the bogie under complex perturbations, different step perturbations are applied to the four magnetic poles at different times, as shown in 7(a), and the attitude information of the bogie is collected as shown in Fig. 7.
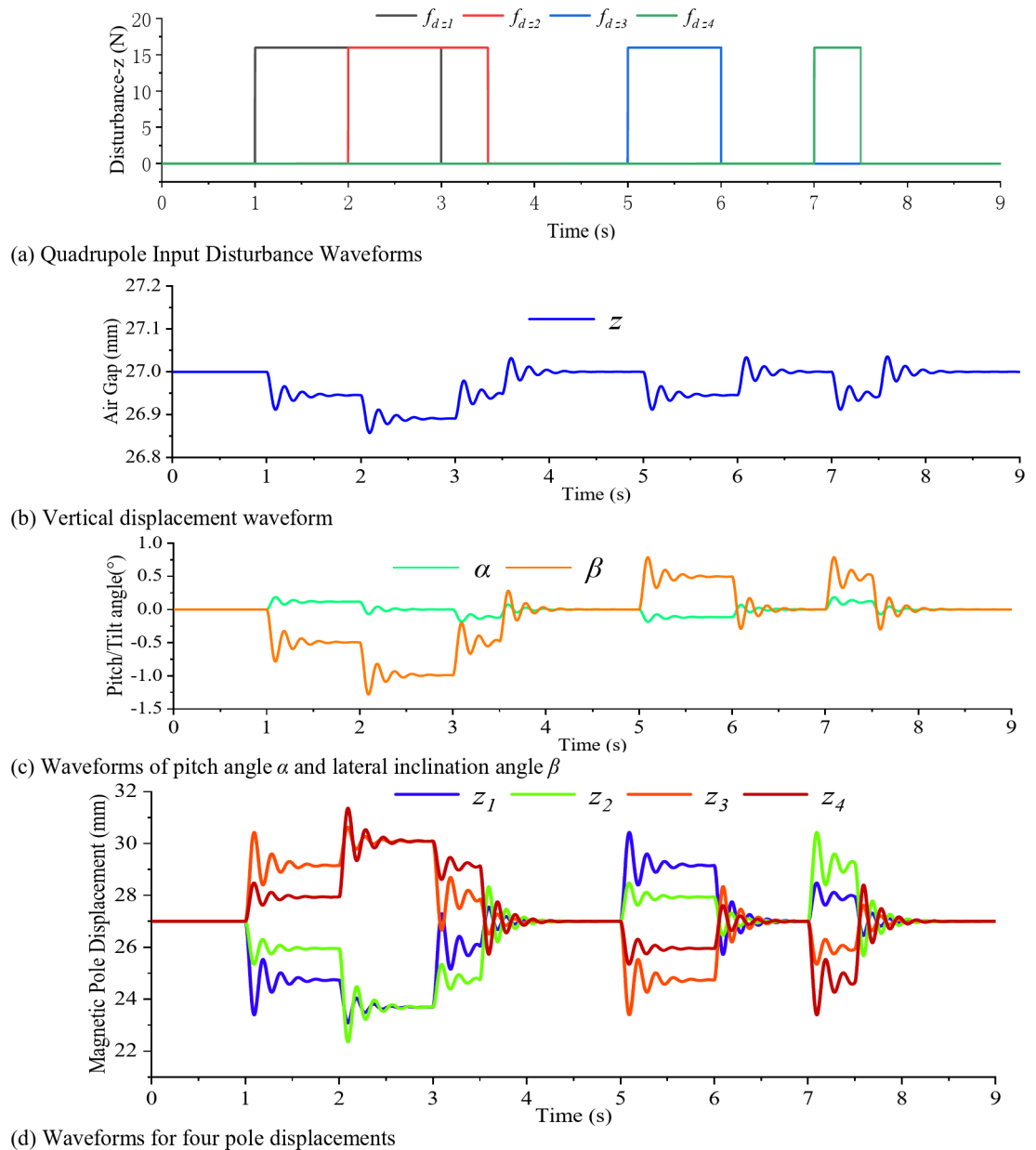
(a) Quadrupole Input Disturbance Waveforms

(b) Vertical displacement waveform

(c) Waveforms of pitch angle α and lateral inclination angle β

(d) Waveforms for four pole displacements

Fig. 7. Waveforms under multiple perturbations.

As shown in Fig. 7, the perturbation is applied only in magnetic pole 1 during 1–2 s. During this period, z appears to fall first and then oscillate with a small amplitude, and finally stabilizes at the position of 26.95 mm, α increases first and then oscillates and stabilizes at about 0.1°, and β decreases first and then oscillates and stabilizes at about -0.5°. The amplitude and law of oscillation of each pole displacement are different, z_1 and z_2 firstly decrease and then oscillate, z_3 and z_4 firstly increase and then oscillate, and the amplitude of oscillation is z_1,z_3, z_2,z_4 in the order of large to small. The minimum values of z_1 and z_2 are about 23.39 mm and 25.35 mm respectively, and the maximum values of z_3 and z_4 are about 30.42 mm and 28.47 mm respectively.

During the period of 2-3 s, both magnetic pole 1 and magnetic pole 2 are perturbed, during this period, z first drops and then oscillates from the position of 26.95 mm, and stabilizes at the position of 26.9 mm at about 2.8 s. α first drops and then oscillates from 0.1°, and finally stabilizes at about 0°, and β continues to drop and then oscillates from the position of -0.5°, and finally stabilizes at about -1°. z_1 and z_2 first drops and then oscillates, and finally Both are stabilized at about 23.72 mm, and the minimum values of z_1 and z_2 are about 23.08 mm and 22.35 mm, respectively. z_3 and z_4 first rise and then oscillate, and both are stabilized at about 30.10 mm, and the maximum values of z_3 and z4 are about 30.63 mm and 31.36 mm, respectively. The amplitude of oscillation of the displacement of the magnetic poles in the order from the largest to the smallest is z_2,z_4, z_1,z_3.

During the 3–5 s period, only the perturbation of magnetic pole 2, z rises and then oscillates from 26.95 mm and finally stabilizes at about 27 mm, α falls and then oscillates, β rises and then oscillates, and finally both stabilize at 0°. Both z_1 and z_2 first rose and then oscillated from the position of 23.72 mm and finally stabilized at
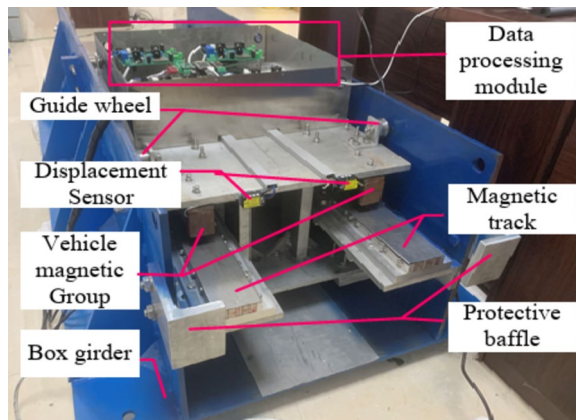
Fig. 8. Experimental platform of permanent magnet magnetic levitation.
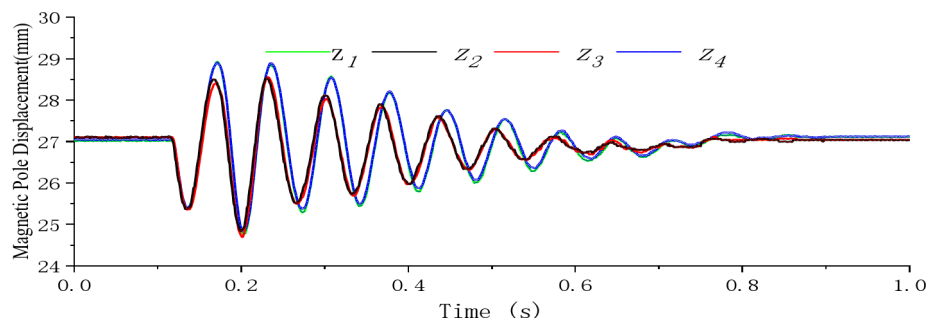

Fig. 9. Waveforms of 4-magnet pole levitation gap variation under z-axis perturbation.

27.00 mm, with maximum oscillations of about 3.57 mm and 2.51 mm, respectively. Both z_3 and z_4 first dropped and then oscillated from the position of 30.00 mm and finally stabilized at 27 mm with maximum amplitudes of about 3.44 mm and 1.49 mm, respectively. During 5-9 s, the dynamic change laws of the bogie is similar to simulation step 2 and will not be repeated.

Experiment

In order to verify the reliability of the theoretical derivation in part 3 and the analog simulation in part 5, a permanent magnet magnetic levitation (PMML) physical experiment platform as shown in Fig. 8 is constructed and physical experiments are conducted.

The elastic ball with weight of 2 kg is used to make a free-fall motion to hit the bogie as a vertical perturbation from 30 mm above the center of the load plate of the bogie at the moment of 0.1 s, and the displacement signals of the four magnetic poles are collected as shown in Fig. 9.

From Fig. 9, it can be seen that the displacements z1-z4 of the four magnetic poles all fall and then oscillate from 27 mm, and return to stability at about 0.8 s. Although there are slight differences in the frequency and amplitude of oscillation, they are relatively close to each other, and match with the simulation results of the step 1 in Section V.

Using the weight of 2 kg elastic ball in 1 s, 4 s, 7 s, 10 s moments from the four magnetic poles directly above the 30 mm to do free-fall motion, respectively, to the 1–4 magnetic poles to apply perturbation, and collect the displacement signal of the four magnetic poles as shown in Fig. 10.

The results in Fig. 10 show that the oscillation frequencies of z_1-z_4 are almost the same during the period of 1–2.5 s. z_1 and z_2 oscillate after decreasing from 27 mm, and z_3 and z_4 oscillate after increasing from 27 mm, and all of them return to stabilization at about 1.7 s. The amplitudes of z_1 and z_2 are close to each other, and the displacements of z_3 and z_4 are slightly higher than those of z_1 and z_2. Because the magnetic pole 1 increases the weight of the ball, the displacements of z_3 and z_4 are slightly higher than those of z_1 and z_2 at the time of regression stabilization. z_1 and z_2 have close amplitudes, z_1 is slightly larger than z_2, and the minimum value of z_1 is about 24.00 mm, z_3 and z_4 have close amplitudes, and the amplitude of z_4 is slightly larger than the amplitude of z_3, and the maximum value of z_4 is about 28.40 mm. In 2.5-4 s, small oscillations occurred in z_1-z_4 as a result of the removal of the perturbing puck. In 4-7 s, the oscillations were similar to those during 1-4 s, so they are not repeated. In 7-10 s, z_1 and z_2 rise and then oscillate, while z_3 and z_4 fall and then oscillate, with z_1 oscillating slightly more than z_2 and z_4 oscillating slightly more than z_3. During 10-12 s, z_1 and z_2 rise and then oscillate, while z_3 and z_4 fall and then oscillate, but the amplitude of the oscillations is larger for z_2 and z_4 than for z_1 and z_3, and the amplitude of the oscillations is larger for z_1 and z_3.
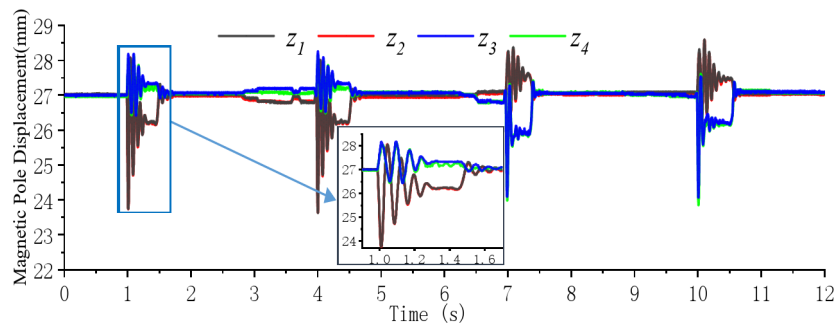
Fig. 10. Suspension gap under 4 magnetic pole perturbation.

The results of the physical experiment are slightly different from the simulation results of step 2 in part 5, but the rule of change basically matches, and the experimental results have a high degree of confidence. There are three reasons for the above results. First, in order to ensure the stable operation of the platform, the guide wheel is added to the physical experiment platform, which restrains the bogie from doing side-tilting movement due to the limiting effect of the guide wheel. Second, it is affected by the processing accuracy of the physics experiment platform. Third, the design of the actual experiment is difficult to be exactly the same as the simulation.

Conclusion

Aiming at the problem of complex dynamic characteristics of permanent magnet magnetic levitation system, this paper explores the levitation mechanism and coupling characteristics of repulsive permanent magnet magnetic levitation system through a combination of theoretical analysis, simulation and physical experiment, and reveals the motion law of the four-magnet pole bogie under the complex perturbation. The following conclusions can be drawn from the theoretical derivation and experimental results analysis.

1. The analytical model of levitation force based on Halbach permanent magnet array is constructed by incorporating the proportional and exponential correction factors of the magnetic induction strength, which can effectively compensate for the levitation force variations caused by the differences in the performance of the permanent magnet materials and fluctuations in the precision of the magnetic track mounting, and it can be adapted to the different and complex working conditions, thus improving the accuracy of the model.
2. By the method of coordinate transformation, the dynamics model of the coupling relationship between the levitation gap of four magnetic poles and three degrees of freedom can be established, which can reveal the coupling mechanism of the permanent magnet magnetic levitation system, and also realize the decoupling of the system input and output.
3. Due to the coupling relationship between the four magnetic poles of the rigid structure bogie, when only the nth ($n = 1,2,3,4$) pole is perturbed, the four poles will undergo oscillatory motions with the same frequency but with different amplitudes, and the oscillatory amplitudes are ranked from the largest to the smallest as $z_{p1}, z_{p3}, z_{p2}, z_{p4}(p_1 = n, p_2 = n + 1, p_3 = n + 2, p_4 = n + 3$,when $p_x \geq 4, p_x = p_x - 4)$.

Data availability

All data generated or analysed during this study are included in this published article.

References
1. Kuang H, Shi M, Zhan P. et al. Vibration characterization of permanent magnet levitation vehicle system based on permanent magnetic track relationships. *Int. J. Struct. Stab. Dyn.* (2024) (prepublish).
2. Zhao, C. et al. Magnetic characterization between on-board permanent magnet and permanent magnet track under five positional parameters. *J. Southwest Jiaotong Univ.* 1–8 http://kns.cnki.net/kcms/detail/51.1277.u.20240517.1210.002.html (2024).
3. Jianhe, Y. et al. Concise magnetic force model for Halbach-type magnet arrays and its application in permanent magnetic guideway optimization. *J. Magn. Magn. Mater.* 587 (2023).
4. Xuesong, Q. et al. Analysis of the magnetic levitation characteristics of the vertical Halbach array in a permanent magnet rotor. *Nonlinear Dyn.* 1–16 (2024) (prepublish).
5. Zhang, H., Kou, B. Q. & Zhou, Y. H. Analysis and design of a novel magnetic levitation gravity compensator with low passive force variation in a large vertical displacement. *IEEE Trans. Ind. Electron.* **67**(6), 4797–4805 (2020).
6. Yao, Q. et al. Fuzzy linear active disturbance rejection control method for permanent magnet electromagnetic hybrid suspension platform. *Appl. Sci.* **13**(4), 2631–2631 (2023).
7. Yongchao, W. et al. Simulation and experimental research on electromagnetic radiation from suspended permanent magnetic levitation train. *Int. J. Appl. Electromagn. Mech.* **70**(2), 129–147 (2022).
8. Wenzhe, P. Research on decoupling control and anti-bias load characteristics of permanent magnetic levitation platform. *Shenyang Univ. Technol.* https://doi.org/10.27322/d.cnki.gsgyu.2022.000567 (2023).
9. Sun, F. et al. Floating control method of variable magnetic circuit type permanent magnetic levitation platform. *J. Southwest Jiaotong Univ.* **57**(03), 531–539 (2022).
10. Chuan, Z. et al. Research of permanent magnetic levitation system: Analysis, control strategy design, and experiment. *Proc. Inst. Mech. Eng. Part C J. Mech. Eng. Sci.* **236**(14), 7617–7628 (2022).

11. Hong, Y. et al. Orientation optimization of the Halbach PMG for the levitation and guidance performance of the HTS maglev system. *Phys. C Supercond. Appl.* **624**, 1354567–1354567 (2024).
12. Halbach, K. Permanent magnets for production and use of high energy beams. In *Proceedings of the 8th International Work Shop on Rare-Earth Permanent Magnets*, 123–136 (1985).
13. Jiang, X. *Modeling and Magnetic Field Analysis of a New Permanent Magnet Motor Based on Halbach Array Pole Structure* (Hefei University of Technology, 2021).
14. Peng, J., Zhao, X. & Guo, Y. Study on the effect of permanent magnet guideway surface defect on the mechanical properties of multi-surface high-temperature superconducting permanent magnet levitation system with Halbach-type guideway. *J. Phys. Conf. Ser.* **2808**(1), 012068–012068 (2024).
15. Chen, J. et al. A magnetic force model study of Halbach array permanent magnet bearing. *J. Harbin Inst. Technol.* **16**(5), 72–76 (2011).
16. Sun, L. & Zhang, T. Research on the mathematical model of permanent magnet magnetic bearing. *J. Mech. Eng.* **41**(4), 69–74 (2005).
17. Hongfu, S. et al. Linear permanent magnet electrodynamic suspension system: Dynamic characteristics, magnetic-mechanical coupling and filed test. *Measurement* **225**, 113960 (2024).
18. Li, C. et al. Optimization of Halbach permanent magnet structure in magnetic levitation train engineering. *J. Eng. Des.* **14**(4), 334–338 (2007).
19. Fang, H. et al. Optimal design of Halbach square array adsorption mechanism. *Mach. Des. Manuf.* **05**, 226–230+234 (2021).
20. Li, L. Suspension rail permanent magnetic double suction balanced compensated suspension road car system: CN1680135A [P] 2005-10-12 (2005).
21. Malewicki, D. J. A retrospective of solid-state transportation systems. *Proc. IEEE* **87**(4), 680–687 (1999).
22. Wiseman, Y. Safety mechanism for SkyTran tracks. *Int. J. Control Autom.* **10**(7), 51–60 (2017).
23. Yang, J. et al. Research and design of permanent magnet magnetic levitation air rail system. *J. Railw.* **42**(10), 34–41 (2020).
24. Gao, T. et al. Design of new energy-efficient permanent magnetic maglev vehicle suspension system. *IEEE Access* **10**, 1–20 (2019).
25. Jiang, Y. et al. Optimization on size of Halbach array permanent magnets for magnetic levitation system for permanent magnet maglev train. *IEEE Access* **10**, 1109–1116 (2021).
26. Zhou, F., Yang, J. & Jia, L. Structure size optimization and magnetic circuit design of permanent magnet levitation system based on Halbach array. *IEEE Access* **11**, 113244–113254. https://doi.org/10.1109/ACCESS.2023.3323596(2023) (2023).

Author contributions

This paper was co-authored by Fazuke Zhou , Jie Yang, Hailin Hu and Tao Gao, with Fazuke Zhou being responsible for the full text, Jie Yang for the overall design and the construction of the physical experimental platform, Hailin Hu for the data acquisition, and Tao Gao for the analog simulation calculations.

Funding

Declarations

Competing interests

The authors declare no competing interests.

Additional information

Supplementary Information The online version contains supplementary material available at https://doi.org/10.1038/s41598-024-81439-2.

Correspondence and requests for materials should be addressed to J.Y.

Reprints and permissions information is available at www.nature.com/reprints.

Publisher's note Springer Nature remains neutral with regard to jurisdictional claims in published maps and institutional affiliations.